HD scattering from Pt(111): Rotational excitation probabilities

James P. Cowin,[a] Chein-Fan Yu, Steven J. Sibener, and Lennard Wharton[b]

The James Franck Institute and The Department of Chemistry, The University of Chicago, Chicago, Illinois 60637
(Received 15 April 1983; accepted 22 June 1983)

We measured the rotationally inelastic diffractive scattering probabilities for an HD beam colliding with a smooth Pt(111) surface. These large $T \rightarrow R$ inelastic probabilities were measured as a function of incidence angle for a 110 meV beam energy. The results are in excellent agreement with a simple physical model of an eccentrically weighted sphere colliding with a hard wall, with an attractive well depth of 55 ± 10 meV. The numerical "GR" method of Garcia and co-workers was found superior to an eikonal method in solving this rotational quantum boundary value problem.

INTRODUCTION

HD scatters from a Pt(111) surface with large rotationally inelastic cross sections. These cross sections were found to vary with incident angle in a generally smooth fashion, modulated by sharp dips and peaks. This paper presents the data and compares the smooth variation of the cross sections to simple dynamical models. The sharp dips and peaks are caused by the previously unobserved phenomenon of rotationally mediated selective adsorption (RMSA).[1-4] This RMSA is a new phenomenon first discovered in this scattering of HD from Pt(111).[1]

There has been much recent interest in rotationally inelastic scattering of diatomics from surfaces.[5] The spectroscopically determined final rotational populations promise to greatly increase our understanding of gas–surface energy transfer. So far, these studies involve NO, CO, and HF. The simpler cases involving light diatomics—H_2, HD, and D_2—have been studied for quite a few years. This has been possible because these molecules have large rotational constants and readily diffract from ordered surfaces. The diffraction kinematics place each distinct rotational energy change into a different final scattering angle.

Most of the prior hydrogen work involved nonmetals; LiF, MgO, and graphite.[6] For these systems, surface corrugation dominates the scattering—greatly complicating the theoretical analysis by raising the number of significant open channels, often to several hundred. Close-packed metal surfaces, with near negligible surface corrugation, should provide far simpler systems. Prior work[7] looked at H_2 or D_2 scattering. These molecules showed weak rotational excitation, due to the small (and theoretically subtle) nonsphericity of the molecule. The nuclear spin statistics further complicate the problem, especially in making it difficult to produce a pure J-state molecular beam.

HD scattering is quite different from either H_2 or D_2 scattering. The rotational coupling is large and known, caused by the shift in the center-of-mass from the HD bond center. This makes HD scattering from close-packed metal surfaces nearly an ideal system. Theoretically, the Hamiltonian should be sufficiently known, and simple enough to be very tractable. Experimentally, the rotationally inelastic cross sections are easily measurable and the pure $J=0$ beams we produce make analysis unambiguous.

In this paper, we report the rotational excitation probabilities (translation rotation) for a $J=0$ beam at 110 meV translational energy, scattering from a Pt(111) surface. Data taken in 5° increments of incident angle are in excellent agreement with predictions based on the physical model of an eccentrically weighted hard-sphere collision, provided that the acceleration caused by the attractive well is included. The "GR" method of Garcia *et al.*[8] was found convenient and numerically superior to the eikonal treatment of Ref. 9 in solving the quantum boundary conditions.

It is interesting to note that HD scattering from Pt(111) was studied over 13 years ago by another group.[10] Had they had a supersonic rather than effusive beam, perhaps many of the current results would have been published much earlier.

The analysis of the RMSA resonances is deferred to a future publication.[4]

EXPERIMENTAL

Apparatus

The apparatus has been described previously.[11] It allows the measurement of the angular and velocity distributions of molecules scattered from a well-characterized single crystal surface. A diagram of it is shown in Fig. 1.

The main chamber is a bakeable UHV system, pumped by a 400 ℓ/s ion pump to a base pressure of about 1×10^{-10} Torr. Mounted inside is a polished Pt(111) oriented crystal, in the form of a 1/4 in. diameter disk. Three degrees of angular adjustment were provided by a crystal manipulator. The crystal was cleaned using intense oxygen baking and ion sputtering treatment, sim-

[a] To whom all correspondence should be directed. Permanent address: Department of Chemistry, University of California, Santa Barbara, CA 93106.

[b] Permanent address: Worthington Division, McGraw–Edison Co., Basking Ridge, NJ 07920.

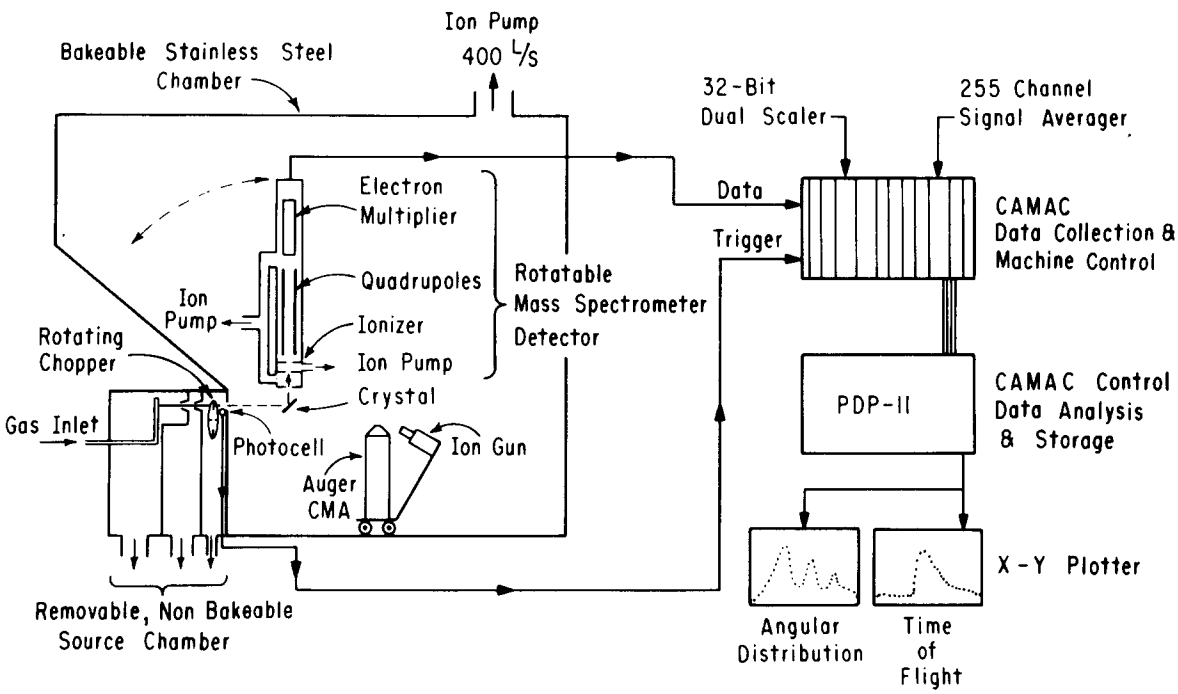

FIG. 1. Experimental apparatus. A schematic diagram of the apparatus and the data taking electronics are shown.

ilar to published procedures.[12] Brief oxygen treatments prior to each day's runs, occasionally with gentle ion sputtering and annealing, consistently produced a well-ordered (indicated by He or HD diffraction) and clean surface (Auger spectrum showing less than 0.01 monolayers of C, O, or Ca, and no detectable Si, P, S, or other contaminants). The surface temperature was varied using resistive heating and/or liquid cryogen cooling. The temperature was monitored with a Chromel/Alumel thermocouple.

A supersonic beam was aimed at the crystal from a demountable source chamber. The beam source had a nozzle diameter of 0.0025 cm and was used with a 200 to 300 psi backing pressure. The nozzle could be heated or cooled, however for the portion of the study presented in this paper, a room temperature nozzle was used. The beam was differentially pumped and collimated to about 0.1°. The beam diameter at the crystal was 0.07 cm.

The HD was produced "on line" by isotopically equilibrating a 4 to 1 $H_2 + D_2$ mixture flowing through a tube packed with Mg at 600 K. At this temperature, magnesium hydride readily equilibrates with gaseous hydrogen. Though possible to chemically produce pure HD from LiAlH and D_2O, the equilibration method was chosen due to its greater simplicity. As well, we found that higher Mach numbers were obtained with an excess of H_2. The 4:1 ratio was a good compromise between Mach number and HD beam intensity.

The intensity and velocity distribution of the incident beam were measured by rotating the mass spectrometer detector to look directly at the beam. A high-speed narrow-slit chopper gave gating for time-of-flight (TOF) measurements. Typically a room temperature nozzle gave HD beams of translational energy 110 meV, mean velocity 0.27×10^6 cm/s, and a Gaussian width of 0.010×10^6 cm/s (speed ratio of 27). The internal vibrational state was nearly completely $\nu=0$ due to the size of $h\nu$ compared to kT. The rotational distribution had relaxed nearly completely (~99%) to $J=0$. This is deduced from the near lack of rotational "hot bands" in the scattering, and confirmed by comparing beam energy to that expected for complete relaxation.

The scattered flux was detected by a rotatable, differentially pumped, quadrupole mass spectrometer. The ionizer was 14.4 cm from the crystal and apertured to 1° resolution. The ions, after amplification with an electron multiplier, could be counted, or measured by analog means. TOF data was collected with a custom-built multichannel scaler. Angular distributions were taken with a dual scaler or via a lock-in amplifier. A PDP-11 computer, through CAMAC interfaces, controlled the beam flag, crystal temperature, detector angle, and data collection and storage.

Procedure

The surface was cleaned by dosing it while at 1000 K with an oxygen beam for 10 to 30 s before each day's runs. The Auger spectrum was rechecked at the end of the day. Carbon buildup was usually 0.01 to 0.02 monolayers. To remove CO and minimize carbon buildup, the crystal was "flashed" to 1050 K for 30 s before each angular distribution run or peak intensity study, and every 10 min thereafter.

The beam intensity and velocity distribution were measured several times a day. The intensity and energy were stable to about 10% and 1%, respectively, over 24 h. To allow good TOF measurements, a special chopper was used. It had two 50% duty cycle slits for angular distribution measurements. The center of the

two "off" quadrants of the blade contained very narrow slits for TOF measurements. A simple digital circuit analyzed the output from the copper monitor photodiode to separate the narrow slit and large slit synch pulses.

Scattered HD angular distributions were measured using the 50% duty-cycle slits at 400 Hz modulation frequency. One counter averaged signal plus background, the other background. Usually 6 s of data collection sufficed for a good signal-to-noise ratio, after which the detector angle was changed by computer control in 0.2° to 1.0° wide steps. The first and last angles taken were the specular reflection, to check for beam drift, contamination, or angular misalignment.

When it was desired to follow a particular inelastic peak over a range of incident angles, a different procedure was used to minimize drift problems. The detector output was routed through an analog amplifier to a lock-in amplifier. The lock-in used as a reference the 400 Hz synch pulse from the chopper photodiode monitor. A 0.1 to 3.0 s time constant was used on the lock-in. The detector was scanned under manual control over the peak of interest. After recording the peak maximum, the crystal angle was changed and the peak scanned again, and so on, until a large range of incident angles had been covered.

A large fraction of a chemisorbed monolayer would form on the platinum surface when dosed with a hydrogen beam while at room temperature. This coverage would interfere with the experiment by greatly attenuating our diffraction peak intensities. To limit the effect to less than 1%, it was necessary to maintain the platinum at 500 K (or higher for temperature studies).

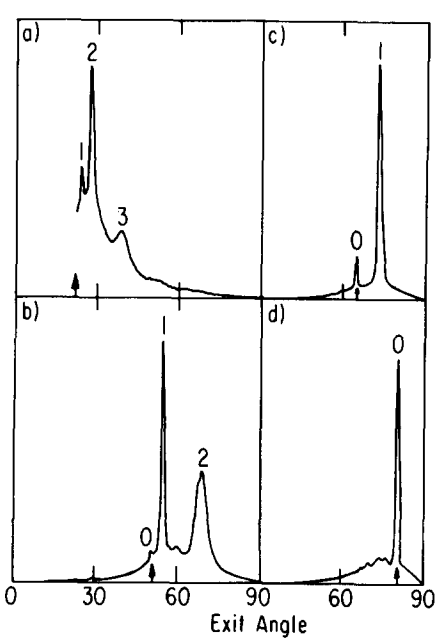

FIG. 2. Typical HD angular distributions. Shown are outgoing HD scattered from a Pt(111) surface at various incidence angles. Surface temperature = 500 K, $\phi = \langle 1,0,-1\rangle$. (a) $\theta_i = 22.5°$, (b) $\theta_i = 50°$, (c) $\theta_i = 65°$, and (d) $\theta_i = 80°$. Vertical axes are in arbitrary units. Labels 0, 1, 2, 3 indicate the final J state of the transition $J = 0 \rightarrow n$ giving rise to the labeled peak.

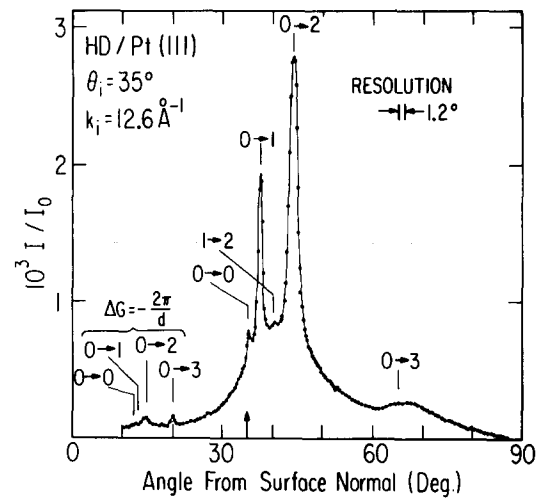

FIG. 3. Assignment of peaks for $\theta_i = 35°$. This is the angular distribution of HD scattered from Pt(111) with $\theta_i = 35°$, $\phi = \langle 1,0,-1\rangle$, $T = 500$ K, beam energy = 109 meV, and surface periodicity $d = 1.385$ Å. Vertical lines give predicted peak positions for the indicated transitions using Eq. (1).

RESULTS–GENERAL ASPECTS

We obtained the scattered HD angular distributions for beams of about 110 meV at incident angles of 22.5°, 25°, 30°, . . . , 85°. A sampling is shown in Figs. 2 and 3. For these, the incident azimuth is $\langle 1, 0, -1\rangle$. The distributions are dominated by several strong peaks, whose number and relation with the specular angle vary with incident angle. This behavior is strikingly different from H_2 or D_2 scattering from metals, which generally shows only one large peak at the specular angle.[10,13] That these HD peaks correspond to rotationally inelastic diffraction is demonstrated by showing that they appear at the angles predicted kinematically.

Conservation of energy and momentum can be shown, in the absence of phonon or other nonrotational energy loss, to lead to a distinct outgoing angle for each rotational transition and diffraction order[14]:

$$\sin^2\theta_f = \frac{(k_i^2 \sin^2\theta_i + G^2 - 2\mathbf{k}_i \cdot \mathbf{G})}{(k_i^2 - \Delta E_{\rm rot}\, 2m/\hbar^2)}, \qquad (1)$$

where $\hbar\mathbf{k}_i$ is the initial HD momentum, θ_i and θ_f are initial and final scattering angles, $\mathbf{G}$ is a surface reciprocal lattice vector which denotes the diffraction order, m is the HD mass, and $\Delta E_{\rm rot}$ is the change in rotational energy (positive for a $J = 0 \rightarrow 1$ transition). Reference 15 gives the geometry necessary to calculate G's, and Table I gives $\Delta E_{\rm rot}$ for $J = 0 \rightarrow J_f$. The peak positions predicted by Eq. (1) are shown in Fig. 3. The agreement is excellent, proving the correctness of the assignment. TOF measurements of the scattered HD directly confirmed this assignment, showing the predicted energy losses. The angular widths, when larger than the 1° detector resolution, are due to the breadth of the incident velocity distributions. According to Eq. (1), each incident velocity within the beam energy spread ($\approx \pm 5$ meV) will scatter to a different final angle. This quantitatively accounts for the peak shapes, as discussed later.

TABLE I. Rotational transition energies for HD (Ref. 16).

J_i	J_f	ΔE_{rot}(meV)	ΔE_{rot}(cm^{-1})
0	0	0.00	0.00
0	1	11.06	89.23
0	2	33.12	267.08
0	3	66.01	532.34
0	4	109.51	883.22
0	5	163.35	1317.42
1	2	22.05	177.85

Nonzero G transitions are also seen in Fig. 2. The weakness of the nonzero-order diffraction shows that the surface potential is only weakly corrugated. This suggests that the effect of surface corrugation on relative rotational excitation probabilities can be largely ignored. This was also concluded in a theoretical study of the much more corrugated H_2–LiF system.[17] This is demonstrated in Fig. 4, where HD scattering at two different azimuths is shown. The major peaks and diffuse background are practically identical. $\phi = \langle 1, 1, -2 \rangle$ shows somewhat larger nonzero-order diffraction than $\phi = \langle 1, 0, -1 \rangle$, due to changes in the length of G and the rougher profile of a close packed plane viewed from $\phi = \langle 1, 1, -2 \rangle$. The intensities of the nonzero-order peaks, summed over J_f, are similar to those for H_2 on Ag(111).[13]

The near negligible effect of surface corrugation means that the x and y (for z perpendicular to the surface) components of energy are nearly conserved, and that only the z component of the incident energy is available for—and capable of influencing—the rotational excitations. This will prove a great simplification for theoretical modeling.

Figures 2 and 3 show very small hot band peaks, principally $J = 1 \rightarrow 2$. We have scattered a beam using a much lower nozzle pressure. The incomplete rotational relaxation under these conditions resulted in $J = 1 \rightarrow 2$, $1 \rightarrow 1$, and $1 \rightarrow 0$ peaks of comparable size to the $J = 0 \rightarrow n$ transition peaks. These results, plus theoretical estimates, show that the hot band and $J = 0 \rightarrow n$ transitions have similar cross sections. Thus we can interpret the smallness of hot band peaks to mean near lack of $J = 0$ in the incoming beam under typical nozzle expansion conditions.

DATA ANALYSIS

The scattered angular distributions need to be analyzed to give the desired rotational excitation probabilities. This is done by fitting them to a theoretically simulated experiment. This requires accurate characterizations of the incoming beam, the apparatus, and the scattering kinematics. Corrections for thermal motion of the lattice and crystal imperfections are also required.

Machine characteristics

A careful analysis of the aperturing of beam and detector, time resolution, etc., indicates that the only significant machine characteristic, when comparing scattered intensities to the direct beam intensity, relate to the chopper gating function and detector resolution. That is, the TOF data of the beam can be simulated by a single convolution of the idealized machine response over the actual chopper gating function, and the outgoing angular distributions can be accurately simulated by a single convolution of the detector angular width (1°) over the idealized machine results for the known beam velocity distribution. The latter depends on the relative constancy of the transition probability over the narrow velocity spread of the beam, which is sufficiently valid for the purpose of this analysis.

Beam analysis

The chopper gating function was measured by slowing the chopper down to 10 RPS. The measured signal with a typical high quality HD beam is a 20X expanded version of the gating function for a 200 RPS chopper. This gating function was very close to the expected results from the system geometry. The beam was modeled by a supersonic shifted Gaussian

$$p(v)dv \propto v^3 \exp[-(v - v_0)^2/\alpha^2]dv \quad \text{(molecules/s)} \qquad (2)$$

with v_0 and α the stream velocity and Gaussian width, respectively. v_0 and α for a typical HD beam were 0.265 and 0.0099 cm/μs, respectively, at 110 meV.

Angular distribution analysis

Because the out-of-plane width of the diffraction peaks are barely wider than the incident beam width, and because the detector engulfs the entire beam when measuring its intensity, the analysis of the in-plane scattering distribution is nearly as simple as writing an ac-

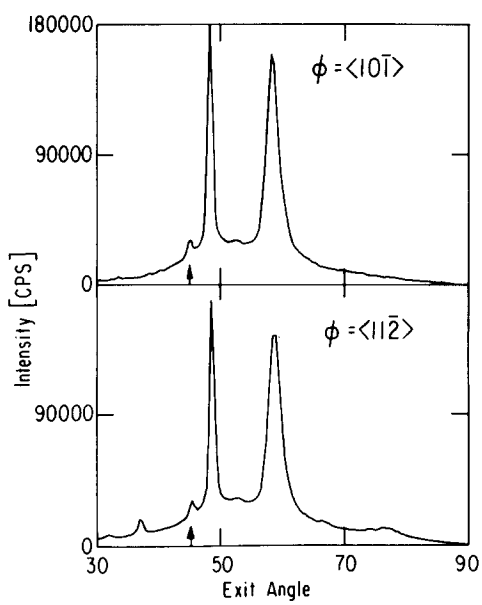

FIG. 4. Azimuthal dependence of HD scattering. Shown is the scattered HD for two different incident azimuths, $\phi = \langle 1, 0, -1 \rangle$ and $\langle 1, 1, -2 \rangle$. $\theta_i = 45°$, beam energy is 111 meV, and $T = 425$ K. The large rotational excitation peaks (zero G vector) and the diffuse background are seen to be practically independent of azimuth.

TABLE II. Rotational excitation probabilities and correction factors at 500 K.

	$P_J(500)$					C_{DW}			
θ_i	$0\to0$	$0\to1$	$0\to2$	$0\to3$	C_{geo}	$0\to0$	$0\to1$	$0\to2$	$0\to3$
20.0	···	···	···	0.00045	1.00	176	146	98.6	53.0
22.5	···	0.00022	0.0012	0.00054	1.00	158	130	88.3	47.3
25	···	0.00030	0.0011	0.00048	1.00	140	116	78.2	41.9
30	···	0.00048	0.0017	0.00060	1.00	107	88.6	59.8	31.8
35	0.00014	0.00118	0.0032	0.0010	1.00	79.8	65.9	44.5	23.5
40	0.00017	0.00187	0.0044	0	1.00	58.2	48.1	32.4	···
45	0.00021	0.0032	0.0069	0	1.00	42.1	34.8	23.4	···
50	0.00015	0.0057	0.0074	0	1.00	30.4	25.1	16.9	···
55	0.00032	0.0147	0.0112	0	1.00	22.2	18.3	12.3	···
60	0.00104	0.021	0	0	1.00	16.5	13.7	···	···
65	0.0022	0.027	0	0	1.00	12.7	10.4	···	···
70	0.0019	0.047	0	0	1.056	10.1	8.3	···	···
75	0.0083	0	0	0	1.236	8.3	···	···	···
80	0.0082	0	0	0	1.649	7.3	···	···	···
85	0.0053	0	0	0	2.028	6.7	···	···	···

curate peak area integration program. A simulation approach is preferred, however, since it allows much more accurate subtraction of incoherent background from the diffraction peak.

The program corrects for the $1/v$ sensitivity of the detector in analyzing inelastic peaks. The linearity of the detector was checked, and found to be better than 10% over the 5 to 1500 μA emission range, under all conditions of count rate, etc., actually used. The crystal viewing factor—the fraction of the beam which actually hits the crystal—was corrected for when appropriate, i.e., $\theta_i \geq 78°$. The detector viewing factor, the fraction of the beam spot on the crystal seen by the detector, was 1.0 for all peaks analyzed here.

Each rotationally inelastic diffraction peak was simulated from the fitted beam parameters, the kinematics of Eq. (1), and a constant transition probability. Where the transition probability is not approximately constant over the beam distribution, the fitted probability will be an average over the beam distribution. The various calculated peak angular distributions are convoluted over the detector resolution, and summed. Due to small errors in beam energy and crystal angle ($\pm 0.1°$), it was necessary to allow the fitting routine to optimize an arbitrary (and small) angular shift for each peak.

The diffuse background was modeled by an orthogonal basis: a Hermite polynomial sum times a Gaussian, in the variable $(\theta_f - \theta_0)/\theta_w$. The Gaussian origin θ_0 and width θ_w, and the polynomial coefficients could be fitted to the experimental background. A Hermite polynomial basis is used for computational convenience, not based on any physical model. This basis is much superior to a sine and cosine basis, because the Gaussian factor allows a natural representation of the monotonically decaying background without tendencies to introduce large spurious oscillations.

Results of angular distribution analysis

Least squares optimization of the fitted parameters was done. Since several parameters were nonlinear, a version of the Marquardt[18] nonlinear-least-squares algorithm was used. When peaks appeared over a particularly wide angular range, the outgoing distribution was split into several sections and fit separately. The peak shapes were almost always fit extremely well. The fitted peaks would be practically indistinguishable from the experimental curves in Fig. 2 had they been included. The only significant deviations in shape were for specular peaks near glacing incidence, which showed slight broadening due to the crystal curvature, and the $J=0\to2$ peaks at 50° and 55°, which showed clefts due to the sharp variation of the probabilities at two resonances. The results of fitting the probabilities for each $J=0\to n$ transition for the 110 meV beams are listed in Table II, as a function of θ_i. The summed probabilities at any incident angle are much less than one in Table II. This is mainly due to two loss mechanisms, Debye–Waller attenuation and the excess geometrical losses. Both are discussed below.

Debye-Waller correction factor

Similar to most other diffractive techniques, molecule–surface diffraction is sensitive to the thermal displacements of the scatterer, causing attenuation of the diffraction peaks. This is particularly true in our experiments, due to the high temperature needed to maintain surface cleanliness. This attenuation is apparent in Fig. 5, where scattered HD angular distributions are shown as a function of temperature between 500 and 1000 K at $\theta_i = 45°$. The aim of treating this attenuation is twofold: First, to provide a formula for empirically extrapolating diffractive probabilities to $T=0$, removing the effects of these thermal displacements; second, to provide estimates of the mean thermal displacement of the surface and the attractive well depth.[19] The results of our analysis, despite some experimental "noise" (Fig. 7), show that the excitation probabilities can be satisfactorily extrapolated to absolute zero. The well depth, within the Beeby model,[19] will be shown to be about 55 ± 10 meV.

Debye–Waller (DW) attenuation for gas–surface scat-

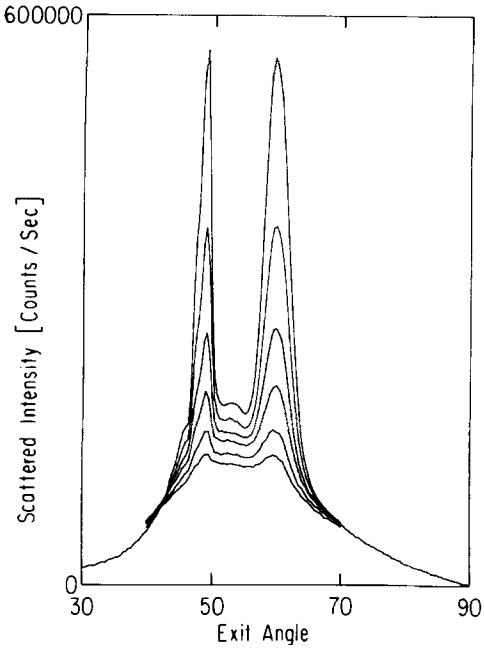

FIG. 5. Surface temperature dependence of HD scattering. The outgoing intensity for HD scattering from Pt(111). $\theta_i = 45°$, $\phi = \langle 1, 0, -1 \rangle$, $E_i = 103.8$ meV. The traces from top to bottom are for surface temperatures of 500, 600, 700, 800, 900, and 1000 K, respectively. The left large peak is $J = 0 \rightarrow 1$, the right one is $J = 0 \rightarrow 2$.

tering has been theoretically treated very carefully recently.[20–22] Their results indicate that many of the simplistic approaches which closely resemble the treatment of x-ray DW attenuation, are qualitatively correct for H_2, HD, D_2, and He diffraction under typical experimental conditions. But the quantitative accuracy and significance of the fitted parameters may be questionable. Forewarned, we will use the simplistic approaches in an empirical manner for temperature extrapolation, and avoid detailed interpretation of the fitted parameters. The simplest form for DW attenuation, borrowed from x-ray theory, has the temperature dependence of the diffractive probability $P(T)$ given by

$$P(T) = P(0) \exp(-\Delta k^2 \langle u_{\Delta k}^2 \rangle) , \qquad (3)$$

where $\Delta \mathbf{k}$ is the change in momentum of the molecule, $\mathbf{u}$ is a thermal displacement of a scatterer, and $\langle u_{\Delta k}^2 \rangle$ is the thermal average of the squared component of $\mathbf{u}$ parallel to $\Delta \mathbf{k}$. The Beeby method[19] treats the effect of the molecule-surface potential by calculating $\Delta \mathbf{k}$ after adding the well depth W to the normal kinetic energy E_z. The variation of $\langle u_{\Delta k}^2 \rangle$ with $\Delta \mathbf{k}$ will be ignored, and for temperatures between about 0.2 and 2 times the Debye temperature it can be treated as proportional to T: $\langle u_{\Delta k}^2 \rangle \approx AT$.[21] This gives for zeroth order diffraction

$$P(T) = P(0) \exp\{-(AT)[(E_i \cos^2 \theta_i + W)^{1/2} + (E_i \cos^2 \theta_i + W - \Delta E_{\rm rot})^{1/2}]^2 2m/\hbar^2\} . \qquad (4)$$

$P(0)$ is the probability in the absence of both thermal and zero-point-motion lattice displacements.

Parameters A and W will be fitted to the temperature dependence of the available sampling of HD diffraction conditions, and will be used to extrapolate all the data to obtain $P(0)$'s. H_2, D_2, and He DW attenuation is also discussed.

The HD data of Fig. 5 and other HD data are presented in Fig. 6. The angular distributions were analyzed as before to give diffraction probabilities. When plotted logarithmically vs T, the data should lie on straight lines according to Eq. (4). The figures show this to be reasonably true, with probably both random and systematic deviations from the line. The fitted slopes appear in Table III. The variation of these slopes with θ_i and $\Delta E_{\rm rot}$ allows a nonlinear least-squares-best fit of A and W to the data. The results appear in Tables III and IV. The standard deviations of the fitted A and W are rather large. The poor fit to the two slopes for $\theta_i = 45°$, $J = 0 \rightarrow 1$ and $\theta_i = 65°$, $J = 0 \rightarrow 0$ is largely responsible; if they are omitted, the fit improves significantly (see Tables III and IV). We will defer further discussion until the related H_2, D_2, and He DW scattering is presented.

H_2 should feel the same surface potential, and have nearly the same A and W as does HD. We measured the variation of the specularly scattered H_2 vs surface temperature, as shown in Fig. 7. Small irreproducibilities are evident where measurements were repeated. The fitted lines allowed A and W to be estimated, based on Eq. (4) (see Tables III and IV). The fitted well depth of 72 ± 6 meV is somewhat deeper than the HD results.

Analysis of the angular dependence of specular scat-

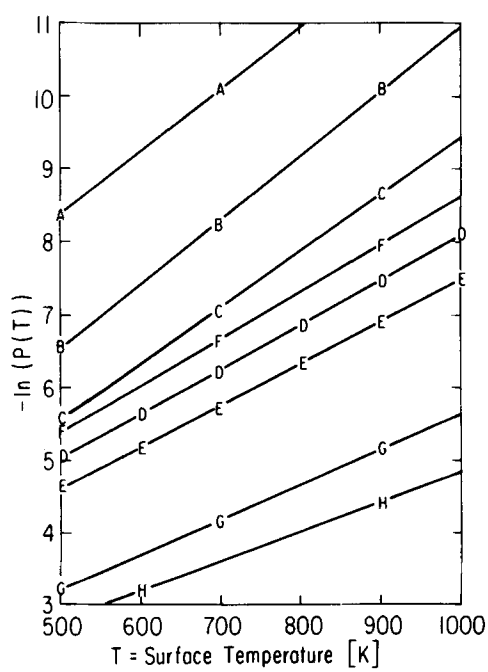

FIG. 6. HD Debye–Waller attenuation. Shown are the logarithms of the probability of HD diffractive rotational excitation vs surface temperature for $\phi = \langle 1, 0, -1 \rangle$ and E_i about 110 meV. Letters A–H denote data points for the following conditions: A, B, C are $\theta_i = 35°$, $E_i = 110.5$ meV, and $J = 0 \rightarrow 0$, 1, and 2, respectively; D, E are $\theta_i = 45°$, $E_i = 103.8$ meV, and $J = 0 \rightarrow 1$ and 2, respectively (plot displaced one unit down for clarity); F, G are $\theta_i = 65°$, $E_i = 110.5$ meV, $J = 0 \rightarrow 0$ and 1, respectively; H is $\theta_i = 80°$, $E_i = 103.7$ meV, $J = 0 \rightarrow 0$. Lines are best fit.

TABLE III. Temperature dependence of logarithm of diffractive probabilities.

Species	E_i (meV)	θ_i	$J=0\rightarrow n$	Plot symbol	$(\hbar^2/8m)d\,\mathrm{Log}[P(T)]/dT$ (10^{-19} cm^2 meV/K)[a] Expt	Pred[1]	Pred[2]	Pred[3]	Pred[4]
H_2	74.0	25	0	a	1.32	1.34	...	...	1.37
H_2	74.0	25	0	c	1.36	1.34	...	...	1.37
H_2	74.0	45	0	d	1.13	1.10	...	...	1.09
H_2	74.0	45	0	e	1.06	1.10	...	...	1.09
H_2	74.0	70	0	f	0.80	0.81	...	...	0.76
H_2	74.0	70	0	g	0.83	0.81	...	...	0.76
HD	110.5	35	0	A	1.49	...	1.50	1.53	1.52
HD	110.5	35	1	B	1.53	...	1.44	1.46	1.46
HD	110.5	35	2	C	1.33	...	1.31	1.32	1.32
HD	103.8	45	1	D	1.04	...	1.20	b	1.20
HD	103.8	45	2	E	0.98	...	1.07	1.06	1.06
HD	110.5	65	0	F	1.11	...	0.91	b	0.88
HD	110.5	65	1	G	0.83	...	0.85	0.81	0.82
HD	103.7	80	0	H	0.70	...	0.73	0.68	0.69
He	64.7	45	...	...	0.56	...	...	...	...

[a]1, 2, 3, 4 refer to models given in Table IV. [b]Purposely omitted for this fit.

tering was not used to estimate DW parameters, given the complications of an angular-dependent sticking probability, and those mentioned by Goodman.[23]

For comparison, the temperature dependence of He DW attenuation was measured at one incident angle and beam energy. Since the incident energy, 64.7 meV, is much larger than the probable He–Pt(111) well depth, a crude estimate of the latter, 9 meV, is sufficient to allow calculation of A.[24] The value of A, determined in Table V, is close to what one would expect using $\langle u_z^2\rangle$ measured for Ag(111)[13] or Cu(100)[25] and rescaling according to the relative Debye-solid parameters. This agreement suggests that there is some validity to our DW measurements.

We find that the temperature dependence of HD and H_2 diffraction are imperfectly given by Eq. (4), either due to limitations of the model of sticking probability effects, and a small amount of experimental irreproducibility. The large spread of fitted A's does not produce such a large spread in DW attenuations, since the fitted W's partially compensate for the differences in A's. Table V shows the reciprocal of the DW attenuation—the DW "correction factor"—for HD scattering at various incident angles. The $W=72$ meV set from the H_2 data, the $W=55$ meV set from the selected HD data, and a set with an unrealistically low W of 25 meV (A best fitted to HD data) are not dramatically different. The $W=55$ and 72 meV factors agree within 5%. The actual well depth ought to lay between 55 and 72 meV.[4] Somewhat arbitrarily, we select the $W=55$ meV set to correct all data to $T=0$, and suggest that the errors will be less than 20%. Further DW studies seem appropriate.

TABLE IV. Fitted Debye–Waller parameters.

Species	Free fit W (meV)	Free fit A (10^{-21} cm^2/K)	Fix $W=55$ meV A (10^{-21} cm^2/K)
H_2 specular	72 ± 6	1.01 ± 0.06 (1)[a]	1.19 ± 0.02 (4)
8 HD peaks	65 ± 17	1.08 ± 0.02 (2)	1.18 ± 0.06 (4)
6 HD peaks	54 ± 7	1.19 ± 0.08 (3)	1.18 ± 0.02 (4)
He specular	(9)[b]	1.37	

[a](1), (2), (3), (4) label parameter sets for Table III.
[b]Assumed.

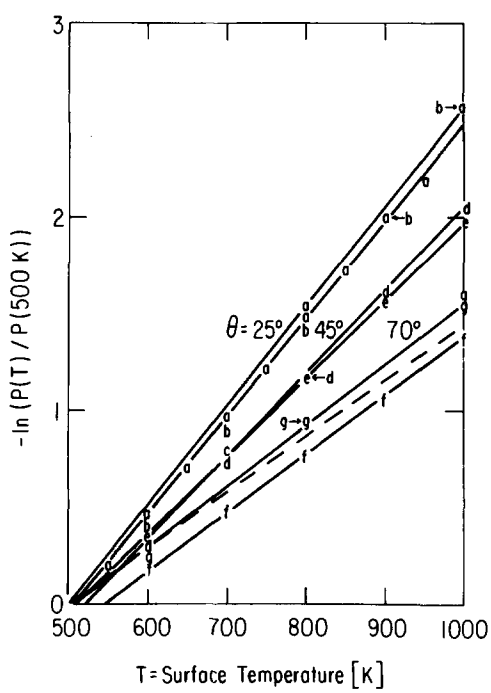

FIG. 7. Debye–Waller plot for specular H_2. $E_i=74.0$ meV, $\theta_i=25°$(a, b, c), 45°(d, e), 70°(f, g). Shown is the variation with surface temperature T of the log of the specular probability relative to that at 500 K. T was sequentially increased for each set, except for b. Solid lines are best fits to each set. Dashed line is that predicted for $\theta_i=70°$ using the constrained fit results from Tables III and IV ($W=55$ meV).

TABLE V. Effect of well depth on Debye–Waller corrections.[a]

		Debye–Waller parameter sets {W (meV), A ($10E-21$ cm^2/K)}		
θ_i	$J=0\rightarrow n$	{25, 1.60}	{55, 1.18}	{72, 1.01}
30	0	143	108	91
30	1	111	89	77
30	2	65	60	55
30	3	26	32	32
50	0	26	31	31
50	1	20	25	26
50	2	11	17	19
70	0	5.8	10	12
70	1	4.4	8.3	10

[a]For $E_i=110$ meV, HD beam, $T=500$ K, using Eq. (4).

Geometrical loss corrections

The studies of the angular dependence of H_2 and D_2 specular scattering, done for DW analysis, revealed attenuation in excess of the DW effect, for $\theta_i > 70°$. This attenuation was found to be independent of mass or energy, strongly suggesting a geometrical origin. The effect of the beam fraction that misses the crystal at large incidence angles, due to its finite width, is insufficient to create the observed attenuation. Monoatomic steps[26] may account for some of this loss. Most probably, this attenuation is caused by the macroscopic crystal curvature near the edges (from polishing). This was apparent both from studying the scattering of laser light and helium beams from the crystal. We found up to 0.4° variation of specular angle from crystal center to edge. The total geometrical loss was well fitted by assuming an effective crystal width of 0.32 instead of 0.68 cm. Correction factors based on this fit appear in Table II, where the ratio of the 0.68 to 0.32 cm crystal attenuation is given. It is assumed here that this is a function of incident angle only.

Corrected probabilities and scattering unitarity

The DW and geometrical loss corrections listed in Table II were applied to the data, and the corrected probabilities are listed in Table VI. Table VI gives our best estimate for the results of scattering from a perfect, motionless Pt(111) surface.

Table VI lists the sum of all rotationally inelastic ($G=0$) probabilities. These sums vary from 0.16 to 0.43, falling quite short of accounting for all the probability. This is serious, both because it suggests that the physics is incompletely understood, and because it complicates comparisons with theories which are unitary. The discrepancy is not likely due to DW theory errors, since the DW correction factors are believed accurate to about 20%, and such errors could not account for the sudden loss of probability seen when a scattering channel closes.

Nonzeroth order diffraction

We have neglected accounting for the probability contained in nonzero **G** diffraction peaks. Figures 4(a) and 4(b) show about 0.01 and 0.10, respectively, for the ratio of nonzero to zero G diffraction probability for in-plane scattering. An estimate for the out-of-plane probabilities is needed. For such a moderately corrugated surface as this is, experience[15] strongly suggests that the diffraction intensity pattern, when viewed in the invariant reciprocal space coordinate system, is roughly independent of incident azimuth for a 45° θ_i. This means that the total nonzero-order diffraction should be roughly three times the sum of that for Figs. 4(a) and 4(b), or 0.32 relative to the zero-order diffraction. The data of Fig. 4 was taken at 425 K where the small amount of adsorbed hydrogen enhances the corrugation. A 500 K surface gives about 0.68 of this intensity in the nonzero-order diffraction, which will reduce the 0.32 to about 0.23. Inclusion of the total nonzero-order diffraction would increase the unitary sum at $\theta_i = 45°$ from about 0.28 to 0.34. We would expect the contribution of the nonzero-order diffraction to be

TABLE VI. Corrected absolute and relative rotational excitation probabilities.

	$P_J(0)$					$P_J(0)/[\Sigma P_J(0)]$			
θ_i	$0\rightarrow 0$	$0\rightarrow 1$	$0\rightarrow 2$	$0\rightarrow 3$	$\Sigma P_J(0)$	$0\rightarrow 0$	$0\rightarrow 1$	$0\rightarrow 2$	$0\rightarrow 3$
20	...	...	...	0.024	...	...	...	...	...
22.5	0.00	0.029	0.104	0.026	0.158	0.00	0.184	0.658	0.165
25	0.00	0.035	0.087	0.020	0.142	0.00	0.246	0.613	0.141
30	0.00	0.043	0.102	0.019	0.164	0.00	0.262	0.622	0.116
35	0.011	0.078	0.144	0.024	0.257	0.043	0.304	0.560	0.093
40	0.010	0.090	0.143	0	0.242	0.041	0.372	0.591	0
45	0.009	0.111	0.161	0	0.281	0.032	0.395	0.573	0
50	0.005	0.143	0.125	0	0.273	0.018	0.524	0.458	0
55	0.077	0.269	0.138	0	0.414	0.017	0.650	0.333	0
60	0.017	0.288	0	0	0.305	0.056	0.944	0	0
65	0.028	0.281	0	0	0.309	0.091	0.909	0	0
70	0.020	0.412	0	0	0.432	0.046	0.954	0	0
75	0.085	0	0	0	0.085	1.00	0	0	0
80	0.099	0	0	0	0.099	1.00	0	0	0
85	0.072	0	0	0	0.072	1.00	0	0	0

similar to this at all the incident angles. The conclusion is that, though significant, the neglected nonzero-order diffraction is only a small part of the missing probability.

Surface imperfections

The surface contains scratches, pits, terrace step edges, and persistent contaminants, which will scatter incoherently any flux which strikes tham. An estimate of this effect can be made using helium diffraction. A 425 K surface typically shows a 0.16 reflectivity for a room temperature supersonic helium beam. Extrapolation to 0 K, as in the Debye–Waller section, gives a reflectivity of 0.83 to 0.99. Thus surface imperfections are not responsible for the large amount of lost flux in this experiment.

Other losses

Multiple-bounce DW attenuation and the sticking probability are most likely responsible for most of the missing probability. The sticking probability, as mentioned in the DW section, could cause tens of percent attenuation. This attenuation would be expected to increase toward the normal,[27] in agreement with the observed trend. However, the sums of Table VI show that as a channel closes down, there is a dramatic loss of probability. This is likely the result of virtual or sometimes real (see Ref. 4) multiple collisions with the surface, as detailed in the scattering theory section. Each collision is likely to suffer multiplicative DW attenuations, which at these surface temperatures, eliminate all but the single collision trajectories from the coherent scattering. Interesting multiple scattering DW effects have been reported for low energy electron diffraction[28]: these studies suggest that much information may be extractable from a careful study of the DW attenuation of HD.

Relative probabilities

The attenuation due to the sticking coefficient is likely to affect all outgoing channels equally. The relative effects of the multiple bounce DW losses is perhaps harder to guess without a detailed theory. This effect is likely to be important only when the coupling to one of these virtual channels is large. At incident angles less than about 45°, the small observed probability for the highest J state that is an open channel $J=3$ suggests that virtual transitions to even higher J states will have negligible influence on the scattering. For the listed angles greater than 70°, there is only one open channel, so there are obviously no effects on relative probabilities there. This leaves only the angular region between 45° and 70° to be considered. Since the transition probabilities back to the open channels $J=0$ and $J=1$ from a virtual $J=2$ state are likely to similar, the loss of these virtual trajectories probably will not greatly alter the relative probabilities of the open channels. This suggests that it is a reasonable (and perhaps the only) choice to compare with theory the relative excitation probabilities. The renormalized probabilities are given in Table VI. They are plotted vs θ_i in Fig. 8.

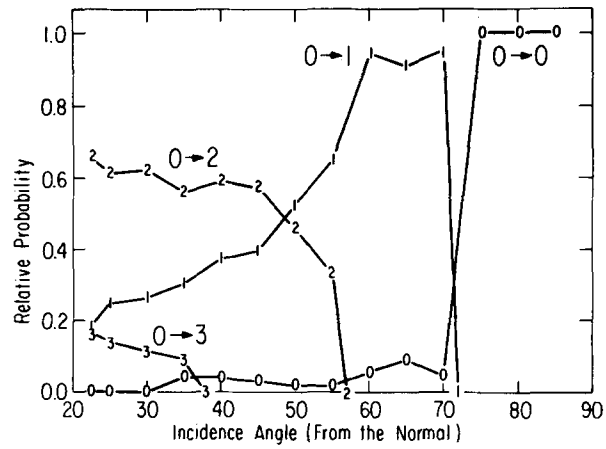

FIG. 8. Relative HD rotational excitation probabilities at 5° increments. Beam energy was about 109 meV, $\phi=\langle 1,0,-1\rangle$. Data was taken at surface temperature = 500 K, but have been corrected for Debye–Waller attenuation, as shown in Tables III and VI. The geometrical losses were also corrected.

COMPARISON WITH THEORY

Applicable theories

Detailed theoretical treatment of all the observed features of the relative rotational excitation probabilities is possible.[3] To be within the scope of this paper, much simpler approaches are required. A number of analytic or computationally efficient treatments of rotational excitation have been developed for surface and gas scattering (see Ref. 17 and references therein[9,29]). In many cases these involve H_2 and its isotopes. These treatments include classical or semiclassical trajectory calculations, eikonal–Raleigh approximations, distorted wave, sudden, and infinite-order sudden approximations. The physics of our system allows major simplification of the Hamiltonian through approximation, while preserving all the essential features of the HD scattering. This Hamiltonian is treated classically, then quantum mechanically by two methods, including the published eikonal–Raleigh method.

Eccentrically weighted sphere model

The surface corrugation plays a very small role in the rotational excitation in scattering from this surface. This is evident from the small size of the nonzero G-vector peaks, the azimuthal invariance of the excitation probabilities, and theoretical and experimental evidence presented in Ref. 17. This means that the scattering potential can be simplified as

$$V(x,y,z,\gamma,\sigma)\approx V(z,\gamma)\ , \tag{5}$$

where x, y, z are the coordinates of the HD center-of-mass and γ and σ are the polar and azimuthal orientation of the molecular axis. This will conserve the x and y components of linear momentum and one component of angular momentum.

H_2 and D_2, for fractional eV translational energy, show little rotational excitation when scattered from a surface or a gas molecule. This implies that the repulsive potential is fairly spherical for H_2 and D_2, and that

the angular-dependent attractive forces are insufficient to induce transitions. This strongly suggests that the rotational coupling for HD will be accurately modeled by a spherical potential, whose center-of-mass has been moved from the center-of-force:

$$V(z,\gamma)=V(z-\delta\cos\gamma)\ , \tag{6}$$

where $\delta=0.12$ Å is the separation between the HD center-of-mass and the center-of-force. The sphere radius is here assumed to be equal to δ. Any other sphere radius would simply add an offset to the z axis, and would not affect the classical or quantum results in any other way. The final approximations involve how the $V(z)$ is treated. The repulsive wall should be responsible for most of the coupling. Since it is steep, it will be approximated as an infinite step at $z=0$. The attractive well will be treated in the Beeby style.[19] The attractive potential is assumed to only increase the z component of the translational energy by the well depth. The particles which undergo a rotational transition that leaves them with insufficient energy to escape this well are assumed (semiclassically) to return to the surface for a second collision. This second collision introduces a second severe Debye–Waller attenuation, preventing these particles from making significant contribution to the coherent scattering.

The sum of these approximations reduces our treatment to the model of a hard eccentrically weighted sphere colliding with a flat surface, a previously applied model.[9] The attractive well effects are simply treated as only increasing the z component of momentum.[19]

Classical treatment

For a molecule colliding with a flat surface, with the molecular axis assumed to lie in the x–z plane, the relevant portions of the Hamiltonian are

$$\begin{aligned} &H=p_z^2/2m+J_y^2/2I+V(z-\delta\cos\gamma)\ ,\\ &V(a)=0\quad\text{for } a>0\ ,\\ &V(a)=\infty\quad\text{for } a<0\ , \end{aligned} \tag{7}$$

with p_z the z component of the momentum, m the HD mass, J_y the angular momentum about the y axis, and I the moment of inertia. The ignored momenta are conserved. For a single impulsive collision with the surface, it is easy to derive from energy, momentum, and angular momentum conservation that

$$p_{zf}=(-p_{zi})(1-C)/(1+C)+J_{yi}\,2(Cm/I)^{1/2}/(1+C)\ , \tag{8a}$$

$$J_{yf}=-(-p_{zi})2(CI/m)^{1/2}/(1+C)+J_{yi}(1-C)/(1+C)\ , \tag{8b}$$

$$C=\delta^2\sin^2(\gamma)m/I\ , \tag{8c}$$

where i and f refer to the initial and final values. For $J_{yi}=0$, the expression for the scattered rotational energy distribution is

$$P(E_{\rm rot})=(1-C^2)/[(E_{zi}+W-E_{\rm rot})\cos\gamma]\ , \tag{9a}$$

$$4C/(1+C)^2=E_{\rm rot}/(E_{zi}+W)\ , \tag{9b}$$

$$0<\gamma<90\ , \tag{9c}$$

where C is calculated from $E_{\rm rot}$ and Eq. (9b), and γ calculated from C and Eq. (8c). The well depth W is shown added to the incident E_z. Figure 9 shows plots of $P(E_{\rm rot})$ calculated for incidence angles of 20° and 40°, for $E_i=110$ meV, and W assumed to be 55 meV. Each distribution has a rotational rainbow and cutoff at a final $E_{\rm rot}$ of $0.4(E_{zi}+W)$. Equation (9) implies that the $J=0\to1$ and $0\to2$ transitions are classically allowed over the entire experimental range (when they are open channels), and that $J=0\to3$ is classically forbidden. This is consistent with the observation of a much lower probability for the latter transition compared to the former two. Note that there are three mechanisms for second encounters between the HD molecules and the surface. The first involves rotational trapping in the attractive well, as discussed earlier. The second mechanism would have the first collision transfering insufficient momentum to reverse the center-of-mass velocity. A third possibility has the molecule moving so slowly away from the surface after the first collision that the eccentrically located hard shell can rotate about the center-of-mass fast enough to collide again. Neither of the latter two can occur (classically) for the parameters appropriate for HD.

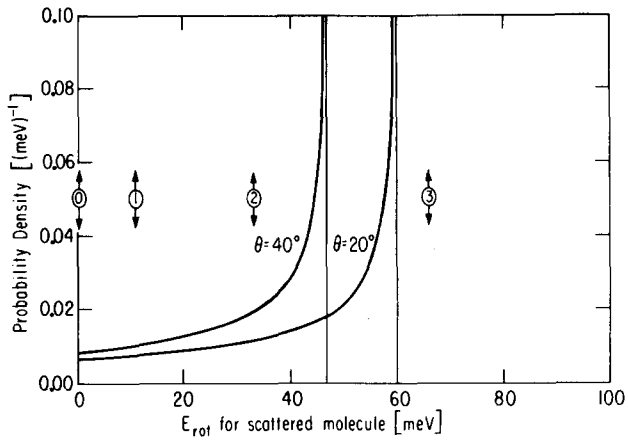

FIG. 9. Classical probabilities. Shown are classical rotational excitation probabilities for eccentrically weighted hard sphere model, Eq. (9). An attractive well of 55 meV is assumed, for $E_i=110$ meV. Probability is plotted vs final rotational energy for initially nonrotating molecule for two incidence angles. Circled numbers give quantized rotational levels of HD.

Quantum treatment (Rayleigh approximation)

The classical Hamiltonian is convertible to quantum mechanics by replacing the rotational energy operator with $J^2-J_z^2$. The potential assures that the rotational quantum number m is conserved. Such a potential invites treatment as a boundary value problem:

$$\Psi(z,\gamma)=0\ ,\quad\text{at } z=\delta\cos\gamma\ . \tag{10}$$

An appropriate expansion of the wave function is

$$\begin{aligned}\Psi(z,\gamma)&=Y_{00}(\gamma)\exp(-ik_i z)\\ &\quad+\sum_J b_J\,Y_{J0}(\gamma)\exp(ik_J z)\ ,\\ k_J&=[k_i^2-J(J+1)m/I]^{1/2}\ ,\end{aligned} \tag{11}$$

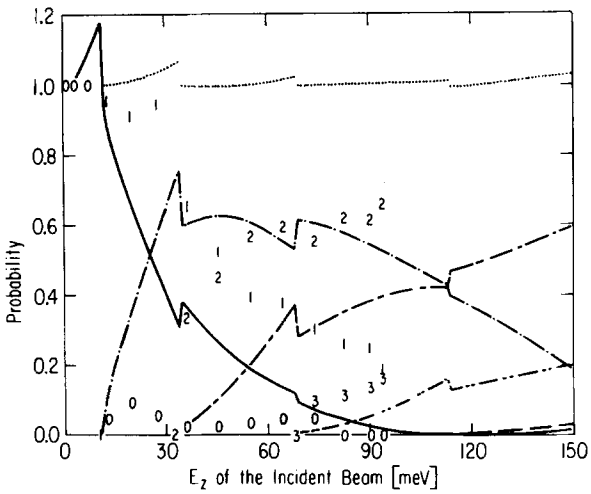

FIG. 10. GR-method solution of the Rayleigh approximation. The GR method of solving the Rayleigh approximated boundary conditions for an eccentrically weighted sphere colliding with a hard wall is shown as a function of the incident z component of energy. No attractive well is included. The dotted curve is the unitary conditions, the solid is the $J=0\rightarrow 0$ probability, the dash-dotted is the $J=0\rightarrow 1$, the dash-short-dashed in the $0\rightarrow 2$, the dash-two-short-dashes is $0\rightarrow 3$, and dashed is the $0\rightarrow 4$. The numbers give the location of the experimentally determined points, the number n referring to the $J=0\rightarrow n$ relative rotational transition probability.

where $Y_{J0}(\gamma)$ is a spherical harmonic, the first term is the incoming wave, and b_J is the coefficient for the Jth scattered wave. For simplicity the z subscripts have been omitted, and the initial rotational level is assumed to be $J=0$. Equation (11) is not valid for $-\delta<z<\delta$, where scattered waves propagating both toward and away from the surface must be used.[30] Extension of the expression in Eq. (11) all the way to $z=\delta\cos\gamma$ is the Rayleigh approximation as applied to surface atom scattering.[8] The Rayleigh approximation should be valid (and usually highly accurate) if, during the collision $(-\delta<z<\delta)$, there is little probability of producing trajectories traveling toward the surface, resulting in a second encounter (distinct from second collisions due to an attractive well). The classical section above showed that the impulsive collision completely reverses the direction of the HD sphere, without second collisions. This suggests that the effects of the neglected waves will be small in the quantum calculation, except when classically forbidden states are being produced with small enough final translational energies to allow a multiple collision through rotation, as mentioned in the classical section. To solve Eqs. (10) and (11), a method borrowed from diffraction will be used. This method will also be compared with a method developed for rotationally inelastic diffraction.

GR-type treatment

Garcia and co-workers developed an efficient method (GR method) of solving a similar Rayleigh boundary equation, where the final states were G-vector diffractive states.[8] Rather than trying to solve Eqs. (10) and (11) by awkward series expansions, as probably could be done, we solved then by the GR method. Transposed to our problem, the GR method starts with truncating the expansion in Eq. (11) at n J states. N equations linear in the b_J are generated by evaluating numerically the spherical harmonics in the expression in Eq. (11) at the boundary [Eq. (10)] for n different γ orientations of the molecule. These linear equations can be solved by standard inversion of a complex matrix. To weight the angle according to the phase space density, equal increments of $\cos\gamma$ were used. The results are shown in Fig. 10 for $n=21$. The number of J states needed increases with the energy. $N=21$ is enough to get near complete convergence up to $E_z=150$ meV. Even when n is reduced to 6, the results are still fairly good even at $E_z=150$ meV, where four states are open. The unitarity shown in Fig. 10 is usually quite close to one, strongly suggesting that the Rayleigh approximation is usually valid. Apparently the Rayleigh method is not valid near the energy when a closed channel is about to open. The worst nonunitary regions are for impact energies less than 33 meV, which will not be needed to compare with the data since the attractive well will assure that the z component of the incident energy is always greater than this.

Comparison with experiment is done for four assumed well depths. For a well of zero depth, the comparison is done in Fig. 10. The experimental points and calculated curves are in poor agreement. A more realistic well depth of 55 meV (from the Debye-Waller analysis) is also tried. This is done by replacing in the calculation E_z with E_z+W. As discussed above, those states with insufficient energy to escape the well are discarded, and the rest of the states renormalized to give a sum of 1. This calculation is compared with the data in Fig. 11(b). The theory and experiment are in remarkably good agreement. The only serious discrepancy is that the predicted $J=0\rightarrow 3$ probability is about 30% to 50% too large. This is at the limit of classical excitability, and may be the most sensitive to the errors in modeling the potential. Also shown are similar comparisons for well depths of 35 meV [Fig. 11(a)] and 75 meV [Fig. 11(b)]. These fits are much poorer than the 55 meV results, and suggests that the real well depth (within the crude treatment here) is perhaps 55 ± 10 meV.

It is interesting to note that newer methods have been developed for G-vector diffraction which retain the efficient numerical technique of the GR method. They remove the Rayleigh approximation, and even include a realistic attractive well.[31] Presumably these same techniques could be applied to HD rotational excitation as well.

An eikonal treatment

It is interesting to compare the GR method for computing rotational excitations under the Rayleigh approximation with another method developed for solving the same equations.[9] The method is an eikonal approximation, depending for its validity on the smallness of $(\delta)\Delta k$ compared to one. It was developed for simultaneous G vector and rotationally inelastic diffraction. Our use involves substituting a surface corrugation of zero am-

plitude into their equations. The results are shown in Fig. 12, compared with the GR method results shown earlier in Fig. 10. The eikonal values have trends similar to the GR values, but the much poorer unitary condition of the eikonal calculation in the region of interest makes the GR method preferable. Interestingly the two methods agree most closely for the smaller energy exchange transitions, where $(\delta)\Delta k$ is smallest.

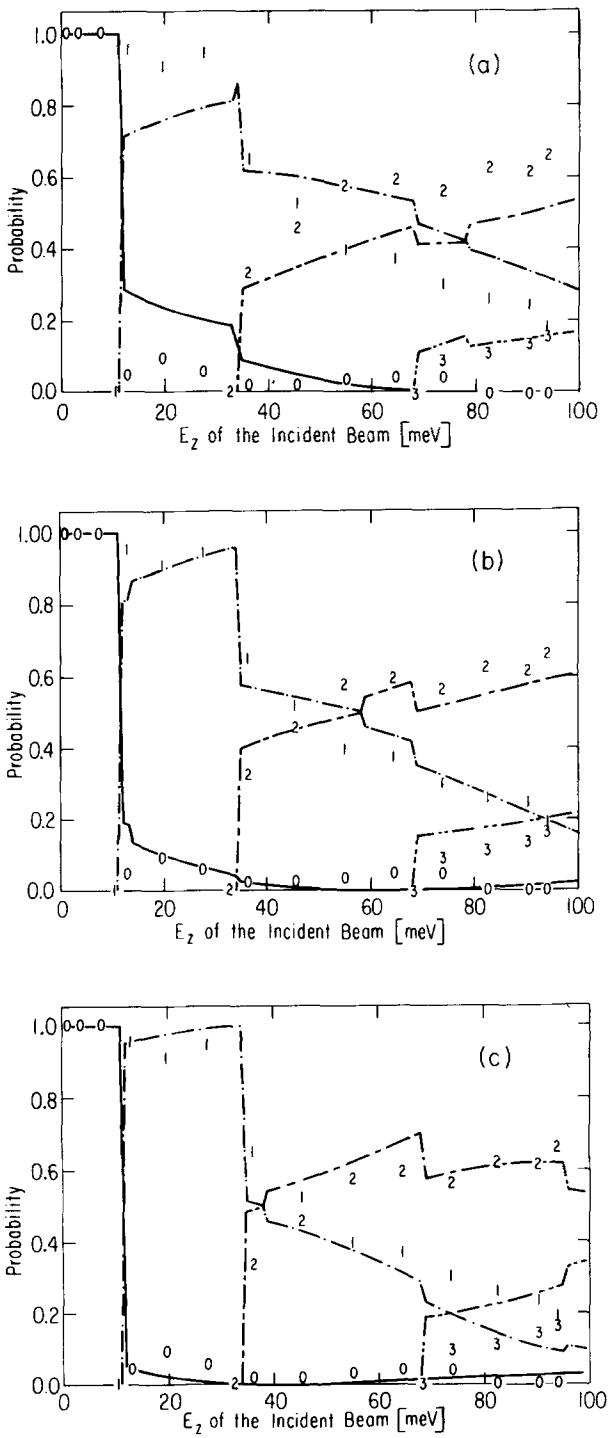

FIG. 11. Comparison of quantum theory excitation probabilities with experiment. The method is the same as for Fig. 10, but with several well depths included: (a) well depth = 35 meV, (b) well depth = 55 meV, (c) well depth = 75 meV.

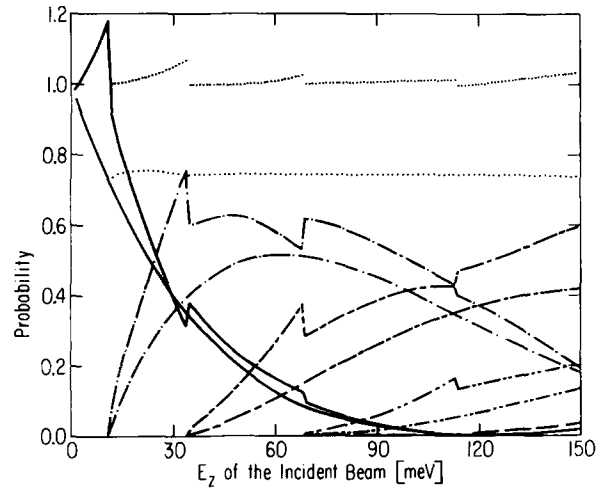

FIG. 12. Eikonal solution to the Rayleigh equation. An eikonal solution to the Rayleigh approximated boundary conditions for an eccentrically weighted sphere colliding with a hard wall is shown as a function of the incident z component of energy. No attractive well is included. The dotted curve is the unitary condition, the solid is the $J=0\rightarrow 1$ probability, the dash-dotted is the $J=0\rightarrow 1$, the dash-short-dashed is the $0\rightarrow 2$, the dash-two-short-dashes is $0\rightarrow 3$, and the dashed is the $0\rightarrow 4$. The GR calculated values are shown for comparison, and are generally larger than the corresponding eikonal values.

CONCLUSIONS

We have shown that HD scattering from smooth metals provides a fairly ideal system for careful comparison of rotational scattering theory with experiment. This is due to the small number of significant open channels (due to the negligible surface corrugation), the simplicity of the coupling Hamiltonian, and the large and easily measured rotational inelastic scattering probabilities. We have found that a quantum treatment of an eccentrically weighted hard-spherical-shell model gives excellent agreement with the experimental data, provided that the acceleration induced by the attractive well is included. The quantum calculation made use of the Rayleigh approximation, and solved the resultant boundary conditions with the convenient GR numerical method,[8] superior to an eikonal treatment[9] of the same equations.

A drawback of this system is the problem of the nonzero sticking probability. This forced the data to be taken at high surface temperature, increasing the errors in correcting for Debye-Waller attenuations. The angular dependent sticking probability was also probably responsible for considerable loss of unitarity. A more inert surface, such as silver, might eliminate this interference.[3]

A new type of resonance in the scattering probability was observed,[1-3] caused by rotationally mediated interactions with quasibound levels of the attractive well. This will be discussed in a later paper.[4]

Finally, we point out that the rotationally inelastic scattering of HD from smooth metals provides a means of producing collimated beams of nearly pure J value, with $m=0$.

ACKNOWLEDGMENTS

This work was supported by the Office of Naval Research grant N00014-77-C-0240; the Air Force Office of Scientific Research, Air Force Systems Command, Director of Chemical Sciences grant #AFOSR 77-3186; and the National Science Foundation grant #DMR 78-14254 and DMR 79-24007. S.J.S. also received support from an Alfred P. Sloan Research Fellowship and a Camille and Henry Dreyfus Young Faculty grant.

[1]J. P. Cowin, C. F. Yu, S. J. Sibener, and J. E. Hurst, J. Chem. Phys. 75, 1033 (1981).

[2]C. F. Yu, C. S. Hogg, J. P. Cowin, K. B. Whaley, J. C. Light, and S. J. Sibener, Isr. J. Chem. **22**, 305 (1982).

[3]K. B. Whaley, J. C. Light, J. P. Cowin, and S. J. Sibener, Chem. Phys. Lett. 89, 89 (1982); R. Schinke, *ibid.* 87, 438 (1982).

[4]J. P. Cowin, C. Yu, S. Sibener, and L. Wharton (to be published).

[5]A. W. Kleyn, A. C. Luntz, and D. J. Auerbach, Phys. Rev. Lett. **47**, 1169 (1981); G. M. McClelland, G. D. Kubiak, H. G. Rennage, and R. N. Zare, *ibid.* **46**, 831 (1981); J. Frenkl, J. Hager, W. Krieger, H. Walther, C. T. Campbell, G. Ertl, H. Kuipers, and K. Segner, *ibid.* **46**, 152 (1981); J. W. Hepburn, F. J. Northrup, G. L. Ogram, J. C. Polanyi, and J. M. Williamson, Chem. Phys. Lett. 85, 127 (1982); D. Ettinger, K. Homma, M. Keil, and J. C. Polanyi, *ibid.* 87, 413 (1982).

[6]R. G. Rowe and G. Ehrlich, J. Chem. Phys. **63**, 4643 (1975); G. Boato, P. Cantini, and L. Mattera, *ibid.* **65**, 544 (1976); L. Mattera, F. Rosatelli, C. Salvo, F. Tommasini, U. Valvusa, and G. Vidali, Surf. Sci. 93, 515 (1980); W. Allison and B. Feuerbacher, Phys. Rev. Lett. **45**, 2040 (1980).

[7]G. Boato, P. Cantini, and R. Tatarek, J. Chem. Phys. **6**, L237 (1976); see also Ref. 13.

[8]N. Garcia, J. Chem. Phys. **67**, 897 (1977).

[9]U. Garibaldi, A. C. Levi, R. Spadacini, and G. E. Tommei, Surf. Sci. 55, 40 (1976).

[10]R. L. Palmer, H. Saltsburg, and J. E. Smith, Jr., J. Chem. Phys. **50**, 4661 (1969).

[11]D. Auerbach, C. Becker, J. P. Cowin, and L. Wharton, Appl. Phys. **14**, 141 (1977); Rev. Sci. Instrum. **49**, 1518 (1978); C. A. Becker, Ph.D. dissertation, University of Chicago, 1980.

[12]J. E. Hurst, D. J. Auerbach, C. A. Becker, J. P. Cowin, K. C. Janda, and L. Wharton, Phys. Rev. Lett. **43**, 1175 (1979).

[13]J. M. Horne, S. C. Yerkes, and D. R. Miller, Surf. Sci. 93, 47 (1980).

[14]F. O. Goodman and H. Y. Wachman, *Dynamics of Gas Surface Scattering* (Academic, New York, 1976).

[15]J. Lee, J. Cowin, and L. Wharton, Surf. Sci. (in press).

[16]H. W. Woolley, R. B. Scott, and F. G. Brickwedde, J. Res. Natl. Bur. Stand. **41**, 379 (1948).

[17]R. B. Gerber, A. T. Yinnon, Y. Shimoni, and D. J. Kouri, J. Chem. Phys. 73, 4397 (1980).

[18]D. W. Marquardt, J. Soc. Ind. Appl. Math. **11**, 431 (1963).

[19]J. L. Beeby, J. Phys. C **4**, L359 (1971).

[20]A. C. Levi and H. Suhl, Surf. Sci. **88**, 221 (1979).

[21]H.-D. Meyer, Surf. Sci. **104**, 117 (1981).

[22]G. Armand and J. R. Manson, Surf. Sci. 80, 532 (1979).

[23]F. O. Goodman, Surf. Sci. **46**, 118 (1974).

[24]J. Lapujoulade, Y. Lejay, and N. Papanicolacu, Surf. Sci. 90, 133 (1979).

[25]J. Lapujoulade, Y. LeCruer, M. LeForte, Y. LeJay, and E. Maurel, Surf. Sci. **103**, L85 (1981).

[26]F. O. Goodman, Surf. Sci. **65**, 37 (1977).

[27]Suggested by microscopic reversibility and the observed $\cos^3(\theta_i)$ desorption pattern. For the latter see: J. E. Smith, R. L. Palmer, J. Chem. Phys. **56**, 13 (1972); J. P. Cowin, C. F. Yu, and L. Wharton (to be published). For more direct evidence, see M. Salmeron, R. J. Gale, and G. A. Somorjai, J. Chem. Phys. **67**, 5324 (1977).

[28]G. Ertl and J. Kuppers, *Monographs in Modern Chemistry* (Chemie, West Germany, 1974), Vol. 4, p. 199.

[29]See these and references cited: M. Faubel and J. P. Toennies, Adv. At. Mol. Phys. **13**, 229 (1977); P. M. Agrawall and M. P. Saksena, J. Chem. Phys. 55, 550 (1976).

[30]G. Armand and J. R. Mason, Phys. Rev. B **19**, 4091 (1979).

[31]See, for example, N. Garcia and N. Cabrera, Phys. Rev. B 18, 576 (1978); and some of their more recent papers, as well as recent work by others.